JAERI-Research
96-047

THE TEM-ACCELERATORS FACILITY AT JAERI-TAKASAKI AND ITS APPLICATION TO MATERIALS SCIENCE

September 1996

Hiroaki ABE, Hiroshi NARAMOTO, Kiichi HOJOU and Shigemi FURUNO

日本原子力研究所
Japan Atomic Energy Research Institute

本レポートは，日本原子力研究所が不定期に公刊している研究報告書です。
入手の問合わせは，日本原子力研究所研究情報部研究情報課（〒319-11 茨城県那珂郡東海村）あて，お申し越しください。なお，このほかに財団法人原子力弘済会資料センター（〒319-11 茨城県那珂郡東海村日本原子力研究所内）で複写による実費頒布をおこなっております。

This report is issued irregularly.
Inquiries about availability of the reports should be addressed to Research Information Division, Department of Intellectual Resources, Japan Atomic Energy Research Institute, Tokai-mura, Naka-gun, Ibaraki-ken, 319-11, Japan.

編集兼発行　日本原子力研究所
印　　刷　いばらき印刷㈱

The TEM-Accelerators Facility at JAERI-Takasaki and its Application to Materials Science

Hiroaki ABE, Hiroshi NARAMOTO, Kiichi HOJOU+ and Shigemi FURUNO+

Department of Material Development
Takasaki Radiation Chemistry Research Establishment
Japan Atomic Energy Research Institute
Watanuki-cho, Takasaki-shi, Gunma-ken

(Received August 6, 1996)

We have developed the transmission/analytical electron microscope interfaced with two sets of ion accelerators (TEM-Accelerators Facility) at JAERI-Takasaki. It consists of a 400 kV analytical and high resolution electron microscope, a 400 kV ion implanter and a 40 kV ion source. The facility is expected to provide quantitative insights into radiation effects, such as damage evolution, irradiation-induced phase transformation and their stability, through in-situ observation and analysis under ion and/or electron irradiation. There are five currently active projects on irradiation effects in inorganic materials: irradiation-induced amorphization in graphite and alumina, ion-beam mixing in metal/silicon bilayers, radiation damage in magnesia and effects of simultaneous irradiation with ions and electrons in magnesia-aluminate spinel. Specifications of the facility is given in detail and the current active research programs are briefly reviewed.

Keywords: TEM, Ion Accelerator, Amorphization, Radiation Damage, Ion-beam Mixing, Graphite, Alumina, Magnesia, Magnesia Aluminate Spinel

---

+ Department of Materials Science and Engineering, Tokai Research Establishment

高崎研究所における加速器結合型電子顕微鏡とその材料科学への応用

日本原子力研究所高崎研究所材料開発部
阿部　弘亨・楢本　　洋・北條　喜一+
古野　茂美+

(1996年8月6日受理)

本論文は高崎研究所イオン照射研究施設（ＴＩＡＲＡ）に設置された加速器結合型電子顕微鏡についての概説である。本装置は400kVイオン注入装置、40kVイオン照射装置、400kV分析電子顕微鏡から構成される。現在、黒鉛のイオン照射誘起非晶質化、アルミナのイオン照射誘起非晶質化、金属／シリコン界面のイオンビームミキシング、マグネシアのイオン照射損傷、マグネシア・アルミナ・スピネルのイオン／電子同時照射効果についての研究を行っている。これらの研究からイオン照射誘起相変態や損傷の蓄積過程には、イオン照射に特徴的なカスケード損傷（はじき出しの密集領域）が大きく影響することが判明した。本稿ではこれらの研究活動についての総説も行う。

高崎研究所：〒370－12　群馬県高崎市綿貫町１２３３
+ 東海研究所材料研究部

Contents

目　　次

1. INTRODUCTION

When materials are subjected to radiation environments, energetic particles transfer their kinetic energy to constituent atoms, introducing atomic displacements, damage cascades (sequences of atomic displacements), electronic excitation and so on. The evolution of such elementary processes of radiation damage dominates changes in physical and chemical properties [1]. Therefore, it is indispensable to obtain information on the damage evolution processes and the resulting radiation-induced phenomena for the development of ion-assisted intelligent materials and of radiation-resistant nuclear materials.

Transmission and analytical electron microscopes (TEM's/AEM's) are the well-known and useful equipment which provides microstructural observation and chemical analysis. Their interfaces with ion accelerators further afford us simultaneous observation and analysis under irradiation with ions and/or electrons [2]. We have developed the TEM/AEM interfaced with two sets of ion accelerators in March 1993 at Takasaki Ion Accelerators for Advanced Radiation Application (TIARA) Facilities [3], JAERI-Takasaki. In the present paper, the in-situ observation and analysis system is described in detail, and its application to studies on irradiation-induced phenomena in ceramics and semiconductors are reported.

2. SPECIFICATIONS OF THE TEM-ACCELERATORS FACILITY AT JAERI-TAKASAKI

The facility consists of a 400 kV ion implanter [3], a 40 kV ion source [4], a 400 kV TEM [4] and their interfaces as shown in Figure 1. The latter two of them were formally installed at JAERI-Tokai and transferred to JAERI-Takasaki in December 1993, and all has been in operation since March 1994. Their specifications are listed in Table 1.

The ion implanter, whose accelerating voltage ranges from 20 to 400 kV, has a

1. INTRODUCTION

When materials are subjected to radiation environments, energetic particles transfer their kinetic energy to constituent atoms, introducing atomic displacements, damage cascades (sequences of atomic displacements), electronic excitation and so on. The evolution of such elementary processes of radiation damage dominates changes in physical and chemical properties [1]. Therefore, it is indispensable to obtain information on the damage evolution processes and the resulting radiation-induced phenomena for the development of ion-assisted intelligent materials and of radiation-resistant nuclear materials.

Transmission and analytical electron microscopes (TEM's/AEM's) are the well-known and useful equipment which provides microstructural observation and chemical analysis. Their interfaces with ion accelerators further afford us simultaneous observation and analysis under irradiation with ions and/or electrons [2]. We have developed the TEM/AEM interfaced with two sets of ion accelerators in March 1993 at Takasaki Ion Accelerators for Advanced Radiation Application (TIARA) Facilities [3], JAERI-Takasaki. In the present paper, the in-situ observation and analysis system is described in detail, and its application to studies on irradiation-induced phenomena in ceramics and semiconductors are reported.

2. SPECIFICATIONS OF THE TEM-ACCELERATORS FACILITY AT JAERI-TAKASAKI

The facility consists of a 400 kV ion implanter [3], a 40 kV ion source [4], a 400 kV TEM [4] and their interfaces as shown in Figure 1. The latter two of them were formally installed at JAERI-Tokai and transferred to JAERI-Takasaki in December 1993, and all has been in operation since March 1994. Their specifications are listed in Table 1.

The ion implanter, whose accelerating voltage ranges from 20 to 400 kV, has a

Freeman type ion source equipped with either an oven or a sputter electrode. Beams are analyzed by a bending magnet, whose mass resolution ($m/\Delta m$) of 100, mounted at the high voltage terminal. The ion beam is, then, transported to a specimen inside the TEM specimen chamber, through a magnet and two sets of electrostatic prisms. One of the electrostatic prisms is located in the TEM specimen chamber, which will be described later. Currently, more than 25 kinds of ions are available, some of which are multiple charged ions; Ar^{2+}, Kr^{2+}, Xe^{2+} and Xe^{3+}, and are metallic elements with high melting points, such as lanthanum and vanadium. Typical flux of ions ranges from 10^{17} to 10^{18} ions/m^2s inside TEM specimen chamber. A beam attenuater, being installed between the high voltage terminal and the magnet in the near future, achieves very low flux such as 10^{14} ions/m^2s.

The 40 kV ion source is of duo-plasmatron type and its accelerating voltage ranges from 2 to 40 kV. The ion beam coming from the ion source is deflected downwards by an angle of 30 degrees with a mass-analyzing magnet and then conducted to the TEM. This system accelerates ions of gaseous elements, such as hydrogen, helium, argon and xenon.

The TEM is an improved version of JEM-4000FX equipped with a parallel detection electron energy loss spectrometer (EELS), an X-ray energy dispersive spectrometer (EDS), a scanning electron microscope (SEM), a scanning transmission electron microscope (STEM) and an in-situ observation and recording system. Spatial or energy resolution is listed in Table 1.

To introduce ion beams inside the TEM, the specimen chamber and the evacuation system has been modified [3,5]. Two sets of electrostatic prisms are installed in specimen chamber so as to lead ion beams to the specimen position as shown in Figure 2. Both ion beams are deflected downwards by 30 degrees by the prisms and injected into specimens through cylindrical aperture of 2 mm in diameter. The prism in the right hand in Figure 2 can deflect ion beams with accelerating voltage up to 300kV. The modified evacuating system [3] consists of an ion pump with titanium sublimation pump and a cryo-cooled diffusion pump. Vacuum level in the specimen chamber is 4×10^{-8} Torr. No contamination of sample was detected at temperature from 90 K to 1200 K under irradiation with ions and electrons.

The ion beam current is measured at specimen position with either of two sets of Faraday cups with an aperture of 0.25 mm in diameter, respectively. One is a specially designed Faraday cup holder and the other is located on a vacuum port at the level of the specimen. The latter one is usually employed for rapid measurement of the ion beam without replacement of the specimen holder with the Faraday cup holder [6]. Other monitors of the ion beam are a Faraday cup at the entrance of TEM specimen chamber and ring-like beam monitors at the entrance and the outlet of the electrostatic prisms.

All of sample holders is compatible with in-situ in irradiation experiments. The sample temperature is controlled from 16 to 1573 K using the holders listed in Table 2. The limit of X-tilt is 25 degrees. The imaging and recording system consists of a CCD camera, a TV monitor and a VTR. The CCD camera is set in slightly oblique direction to electron beam, besides the EELS is at the bottom of microscope column. The images are recorded with the VTR, whose time resolution is 1/30 sec.

The purpose of the second part of this paper is to describe briefly several specific current applications of the facility in materials research. There are five currently active projects as follows: irradiation-induced phase transformation including amorphization [7-9] and ion beam mixing [10]; radiation damage in ceramics [11] including effects of simultaneous ion and electron irradiation [12], and general defect analysis. Three of these projects are collaboration with non-JAERI organization, while two involve JAERI personnel only.

3. AMORPHIZATION, PHASE TRANSFORMATION AND THEIR STABILITY IN CERAMICS AND SEMICONDUCTORS

Graphite is the covalent material consisting of low-Z element and is amorphized at relatively low temperature under irradiation even with light elements. Ion irradiation induces bunches of atomic collision, so-called damage cascades, whose nature, such as their volume and local density of point defects within the regions, is dominated by the combination of projectiles and target. Although damage cascades leave such

The ion beam current is measured at specimen position with either of two sets of Faraday cups with an aperture of 0.25 mm in diameter, respectively. One is a specially designed Faraday cup holder and the other is located on a vacuum port at the level of the specimen. The latter one is usually employed for rapid measurement of the ion beam without replacement of the specimen holder with the Faraday cup holder [6]. Other monitors of the ion beam are a Faraday cup at the entrance of TEM specimen chamber and ring-like beam monitors at the entrance and the outlet of the electrostatic prisms.

All of sample holders is compatible with in-situ in irradiation experiments. The sample temperature is controlled from 16 to 1573 K using the holders listed in Table 2. The limit of X-tilt is 25 degrees. The imaging and recording system consists of a CCD camera, a TV monitor and a VTR. The CCD camera is set in slightly oblique direction to electron beam, besides the EELS is at the bottom of microscope column. The images are recorded with the VTR, whose time resolution is 1/30 sec.

The purpose of the second part of this paper is to describe briefly several specific current applications of the facility in materials research. There are five currently active projects as follows: irradiation-induced phase transformation including amorphization [7-9] and ion beam mixing [10]; radiation damage in ceramics [11] including effects of simultaneous ion and electron irradiation [12], and general defect analysis. Three of these projects are collaboration with non-JAERI organization, while two involve JAERI personnel only.

3. AMORPHIZATION, PHASE TRANSFORMATION AND THEIR STABILITY IN CERAMICS AND SEMICONDUCTORS

Graphite is the covalent material consisting of low-Z element and is amorphized at relatively low temperature under irradiation even with light elements. Ion irradiation induces bunches of atomic collision, so-called damage cascades, whose nature, such as their volume and local density of point defects within the regions, is dominated by the combination of projectiles and target. Although damage cascades leave such

characteristic spatial distribution of point defects, it is uncertain that the effect of damage cascades on the irradiation-induced amorphization. The purpose of this work is to clarify the effects of damage cascades on the amorphization in graphite [7,8]. Selected area electron diffraction technique was taken to confirm the crystalline-to-amorphous transformation. Figure 3 shows an example of the amorphization process induced by irradiation with 40 fJ (250 keV) carbon ions. A diffuse halo ring, associated with the presence of amorphous regions, appeared with irradiation time, while the intensity of the diffraction spots from the remaining crystalline regions decreased and eventually disappeared. Dose-to-amorphization in displacement per atoms (dpa) is defined as the dose at which the diffraction spots disappear and only the halo ring is observed. Figure 4 shows temperature, mass of projectile and energy dependence of the dose-to-amorphization, which was found to vary exponentially with temperature, and shows the apparent threshold temperature for each irradiation condition. Note that the dose increases with temperature in two stages; stage I (<400K) and II (>400K). The apparent threshold temperature increases with increase in mass of projectiles and with decrease in energy of Ar ions. Dose rate dependence of the dose-to-amorphization under irradiation with electrons was observed above 400 K, which corresponds to stage II. The apparent threshold temperature increased with dose rate of electrons and 300 keV argon ions. No amorphization was detected above 860 K. The stage I defect annealing is speculated to be associated with the recombination of vacancies and interlayer carbon molecules (C_2) [13]. Temperature from 400 K to 860 K (stage II), on the other hand, corresponds to the temperature at which carbon molecular clusters ($(C_2)_n$) decompose to molecules permitting their recombination with vacancies [14]. Damage cascades leave high density of point defects which easily results in dense vacancies and the larger molecular clusters, presumably forming stable amorphous clusters (regions) under irradiation at high temperature. Rough estimation of the activation energy for stage I and II defect annealing is 0.17 ± 0.02 eV and 0.24 ± 0.06 eV, respectively, though further discussion on the estimation is required.

Alumina is recognized as one of radiation-resistant materials. Recently, it is reported that irradiation with ions induces amorphization in alumina at liquid nitrogen temperature [15] and at room temperature [16]. Not only the accumulation of

radiation damage but the effect of implanted ions is presumed to be responsible for the amorphization. We have been performing irradiation experiments in thin film alumina at temperatures lower than 300 K and getting the following results [9]. Amorphization was detected at temperatures from 90 K to 160 K under irradiation with 144 fJ (900keV) xenon ions, 96 fJ (600 keV) xenon and 96 fJ (600 keV) krypton ions but with 48 fJ (300 keV) argon ions nor with 48 fJ (300 keV) oxygen ions. Figure 5 shows temperature dependence of the dose-to-amorphization in alpha-alumina irradiated with 144 fJ (900keV) Xe^{3+} or 96 fJ (600 keV) Kr^{2+} ions. One can see that the dose-to-amorphization at 90-160 K was about 3 and 4 dpa under irradiation with xenon and krypton ions, respectively, while at 160-220 K about 8 dpa. No amorphization was observed at temperature higher than 240 K, whilst amorphous-to-crystal transformation was induced. Since defects in alumina are immobile at the temperatures below 450K [17], the amorphization is not induced by atomic diffusion but dominated by accumulation of lattice defects. The difference in the dose-to-amorphization at temperature from 90 to 160 K under ion irradiations is presumed to be attributed to difference in point defect distribution in individual cascades. The individual cascades produced by heavy ions fill a large portion of the transport cascade volume, and vice versa [18]. In other words, heavy ions produce damage cascades with high energy density, the regions of which 'melt' for a very short period (picoseconds) and effectively leave amorphous regions. Only one evidence [19] reported the decrease in luminescence intensity assigned as F_2 centers or divacancies at temperatures 100-350K. The increase in dose-to-amorphization at temperature higher than 160 K in figure 5 may be caused by the annihilation of divacancies in damaged crystal. Further experiments are currently scheduled; temperature and projectile dependence of the dose-to-amorphization in metal/alumina bilayers or in alumina implanted with metallic ions to reveal the chemical effect of implanted/mixed atoms themselves on the irradiation-induced amorphization in alumina will be revealed.

Ion beam mixing is the method that enhances atomic diffusion by irradiation in bi- or multilayers and may form thermally unstable phases in the materials at quite low temperature. Molybdenum silicide is one of the expected electrode materials in semiconductor industries, and its synthesis at low temperature is requested. The ion

beam mixing is applied to synthesize molybdenum silicide in this work. Mo/Si bilayer was irradiated with 192 fJ (1.2 MeV) gold and 28.8 fJ (180 keV) argon ions at room temperature [10]. The initial thickness of Mo is about 60 nm, much smaller than the ranges of ions. Amorphization starts at the interface of the bilayer, while Mo layer retains its crystallinity. EDS results indicate the concomitant mixing of Mo and Si is responsible for the amorphization at the interface. The mixing efficiency under irradiation with gold ions was much greater than that with argon ions, resulting in the formation of amorphous $Mo_{50}Si_{50}$ layer. The results are consistent with size of damage cascades and number and spatial distribution of point defects within cascades. High dose irradiation with argon ions, on the other hand, results in the formation of bubbles, restraining ion beam mixing.

4. RADIATION DAMAGE UNDER IRRADIATION WITH IONS AND/OR ELECTRONS IN CERAMICS

Ceramics is the expected insulators as windows for rf heating in nuclear fusion reactors. Currently, understanding of radiation damage in such ceramic materials is not sufficient because of the complicated characteristics of ceramics; atomic bonding and electrical neutrality for instance. We have performed in-situ observation of loop nucleation and growth processes under irradiation with various kinds of ions (He^+, C^+, O^+, Mg^+, Ar^{2+}, Xe^{2+} with energies of 32-96 fJ (200-600 keV)) in magnesia at relatively high temperature (770-1070 K), and observed nucleation and growth processes of dislocation loops [11], whose nature is 1/2<110>{110} interstitial type. Figure 6 shows microstructural evolution of dislocation loops under irradiation with 16 fJ (100 keV) O^+ ions. Loops appeared in transmission electron microscopy and increased in number at the early stage of irradiation and grew in size gradually with irradiation time. The loops were observed even in thin regions (35-70 nm), where no loop was observed under electron irradiation. Figure 7 shows the variation in loop density against irradiation dose in dpa. Results of the electron irradiation [20] are also shown in the figure for comparison. Loops appear after irradiation at doses such as 0.007 dpa

beam mixing is applied to synthesize molybdenum silicide in this work. Mo/Si bilayer was irradiated with 192 fJ (1.2 MeV) gold and 28.8 fJ (180 keV) argon ions at room temperature [10]. The initial thickness of Mo is about 60 nm, much smaller than the ranges of ions. Amorphization starts at the interface of the bilayer, while Mo layer retains its crystallinity. EDS results indicate the concomitant mixing of Mo and Si is responsible for the amorphization at the interface. The mixing efficiency under irradiation with gold ions was much greater than that with argon ions, resulting in the formation of amorphous $Mo_{50}Si_{50}$ layer. The results are consistent with size of damage cascades and number and spatial distribution of point defects within cascades. High dose irradiation with argon ions, on the other hand, results in the formation of bubbles, restraining ion beam mixing.

4. RADIATION DAMAGE UNDER IRRADIATION WITH IONS AND/OR ELECTRONS IN CERAMICS

Ceramics is the expected insulators as windows for rf heating in nuclear fusion reactors. Currently, understanding of radiation damage in such ceramic materials is not sufficient because of the complicated characteristics of ceramics; atomic bonding and electrical neutrality for instance. We have performed in-situ observation of loop nucleation and growth processes under irradiation with various kinds of ions (He^+, C^+, O^+, Mg^+, Ar^{2+}, Xe^{2+} with energies of 32-96 fJ (200-600 keV)) in magnesia at relatively high temperature (770-1070 K), and observed nucleation and growth processes of dislocation loops [11], whose nature is 1/2<110>{110} interstitial type. Figure 6 shows microstructural evolution of dislocation loops under irradiation with 16 fJ (100 keV) O^+ ions. Loops appeared in transmission electron microscopy and increased in number at the early stage of irradiation and grew in size gradually with irradiation time. The loops were observed even in thin regions (35-70 nm), where no loop was observed under electron irradiation. Figure 7 shows the variation in loop density against irradiation dose in dpa. Results of the electron irradiation [20] are also shown in the figure for comparison. Loops appear after irradiation at doses such as 0.007 dpa

for 48 fJ (300 keV) He^+ irradiation, 0.006 dpa for 48 fJ (300 keV) O^+ and 0.015 dpa for 96 fJ (600 keV) Ar^{2+}, besides 0.09 dpa for 160 fJ (1 MeV) electrons. The loop density varies in proportion to some power, n, of the dose at the early stage of irradiation. The value of n is ~1/2 for 48 fJ (300 keV) He^+ and O^+ irradiation and ~1 for 16 fJ (100 keV) O^+ and 96 fJ (600 keV) Ar^{2+} at 1073 K, besides n~0 for electron irradiation. The size of dislocation loops is also followed the power law. The value of n is 1/2~2/3 at temperature above 900 K and <1/4 below 900 K, much smaller than the values for electron irradiation [20]. It is speculated that dislocation loops nucleate inside or at the periphery of cascade regions under ion irradiation. Further results on temperature, projectile and dose rate dependence of loop density and size will reveal the kinetics of point defects associated with damage cascades in magnesia.

One of indispensable phenomena in damage evolution processes in fusion reactor materials is the simultaneously overlapping effects of ionizing and displacive irradiations. The purpose of this topic [12] is to clarify the effect of simultaneous irradiation with ion beam and the focused electron beam; in the experiments, ratios of electronic to nuclear stopping powers (S_e/S_n) is arbitrarily set. Results are summarized as follows. Void formation was observed under irradiation with 48 fJ (300 keV) He^+ and 32 fJ (200 keV) electrons in magnesia aluminate spinel. Size of the voids in the area irradiated with helium and electrons (S_e/S_n =720) is much larger than the one in the area irradiated with helium ions (S_e/S_n =150). Loop nucleation was observed under irradiation with 48 fJ (300 keV) O^+ (S_e/S_n =6), besides the formation of loops was suppressed under irradiation with oxygen and 32 fJ (200 keV) electrons (S_e/S_n =140). Diffusion of cations towards outside the focused electron beam causes enrichment of cation vacancies inside the electron beam, being attributable for the formation of voids and the suppression of loop nucleation.

5. CONCLUSIONS

A new facility for in-situ observation and analysis under irradiation with ions and electrons was installed, consisting of 400 kV TEM/AEM, 400 kV ion implanter and 40 kV ion source. The specifications of the facility are reviewed. The application to studies on the effects of irradiation with ions and/or electrons reveals:

(1) Damage cascades produce rather stable amorphous clusters, and their accumulation induces amorphization in graphite and alumina;

(2) Synthesis of amorphous $Mo_{50}Si_{50}$ was confirmed under irradiation with 192 fJ (1.2 MeV) gold ions, and damage cascades are presumed to have important role for the ion-beam mixing;

(3) Dislocation loops were observed at the early stage of irradiation with ions even in thin region in magnesia, indicating cascade-enhanced loop nucleation, and

(4) High values of S_e/S_n in magnesia aluminate spinel result in the formation of voids and suppression of loop nucleation under irradiation with electrons and ions.

The authors would like to thank Prof. Kinoshita at Kyushu University, Prof. Ohnuki at Hokkaido University and their coworkers for their kindly providing their experimental results.

REFERENCES

[1] for example, J. Nucl. Mater. 216 (1994).

[2] for example, T. Takeyama, S. Ohnuki and H. Takahashi, J. Nucl. Mater. 133&134 (1985) 571, A. Taylor, C. W. Allen and E. R. Ryan, Nucl. Instrum. Methods B24/25 (1987) 698, and C. Kinoshita, H. Abe, K. Fukumoto, K. Nakai and K. Shinohara, Ultramicroscopy 39 (1991) 205.

[3] Y. Saitoh et al., Nucl. Instrum. Methods B89 (1994) 23.

[4] S. Furuno, K. Hojou, H. Otsu, T. A. Sasaki, K. Izui, T. Tsukamoto and T. Hata, J. Electron Microscopy 41 (1992) 273.

[5] The condenser mini-lens in Figure 2 has also modified to put the electrostatic prism in the right hand inside the specimen chamber.

[6] Typically, it takes about twenty minutes for heating holders to cool the specimen and about an hour for cooling holders to warm it up, while less than a minute to replace sample holders with the Faraday cup located on the vacuum port at the level of the specimen.

[7] H. Abe, H. Naramoto and C. Kinoshita, Mat. Res. Soc. Symp. Proc. 373 (1994) 383.

[8] H. Abe, H. Naramoto, A. Iwase and C. Kinoshita, to be submitted in Tenth International Conference on Ion Beam Modifications of Materials (IBMM-96).

[9] H. Abe, S. Yamamoto and H. Naramoto, to be submitted in Tenth International Conference on Ion Beam Modifications of Materials (IBMM-96).

[10] N. Kawakami, S. Ohnuki, T. Suda and H. Abe, private communication.

[11] K. Sonoda, H. Abe, C. Kinoshita and H. Naramoto, to be submitted in Tenth International Conference on Ion Beam Modifications of Materials (IBMM-96).

[12] K. Yasuda, Y. Watanuki, C. Kinoshita and H. Abe, Ann. Rep. HVEM Lab., Kyushu University 19 (1995) 11.

[13] T. Iwata and H. Suzuki, Proc. Symp. on Rad. Damage in Solids and Reactor Materials, IAEA, Vienna (1963), and B.T. Kelly, 'Physics in Graphite' (Applied Science Publishers Inc., 1981) p.405.

[14] T. Iwata, J. Nucl. Mater. 133&134 (1985) 361.

[15] H. Naramoto et al., to be submitted.

[16] E.D. Specht, D.A. Walko and S.J. Zinkle, Nucl. Instrum. Methods B84 (1994) 323.

[17] G. P. Pells, J. Am. Ceramic Soc. 77 (1994) 368.

[18] J. F. Ziegler, J. P. Biersack and U. Littmark, "The stopping and range of ions in solids" (Pergamon, 1977).

[19] L. S. Welch, A. E. Hughes, G. P. Pells, J. Phys C13 (1980) 1805.

[20] C. Kinoshita, K. Hayashi and T.E. Mitchell, Advances in Ceramics 10 (1985) 490, and Nucl. Instrum. Methods B1 (1984) 209.

Table 1. Equipment specifications

TEM		JEM-4000FX [1]
Voltage		80 - 400 kV
Energy stability		$1x10^{-6}$
Current density		typically $<10^5$ A/m^2
Resolution		0.14-nm lattice
Evacuation		StarCell (230 l/s, Varian Ltd.) , Diffstak (230 l/s, Edwars Ltd.)
		--- specifications ---
Attachments	EELS [2]	1.2 eV (FWHM at zero loss peak, 1mmϕ aperture, 400kV)
	EDS [3]	165 eV (FWHM at Mn-Kα (5.89 keV))
	SEM [1]	2 nm (400 kV operation)
	STEM [1]	2 nm (400 kV operation)
	CCD camera [2]	
	VTR (S-VHS)	

Accelerators	Implanter [4]	Accelerator [5]
Voltage	20 - 400 kV	2 - 40 kV
Energy stability	$3x10^{-3}$	-
Current Density	< 10 A/m^2 for Ar^+ ions	< 2.5 A/m^2 for He^+ ions
Ion sources	Freeman PIG	duoplasmatron
Evacuation	turbo pumps, ion pumps	Diffstak (120 and 230 l/s, Edwards)
Attachments	a beam profile monitor (NEC)	

1) JEOL Ltd., 2) Gatan Inc., type 666, 3) Noran Inc., 4) Nisshin Ltd., 5) Origin Elec. Ltd.

Table 2. Specimen holders for the TEM

Type	Y-tilt / degrees	Temperature / K
Double-tilt [1]	±45	ambient
Double-tilt, beryllium [2]	±20	ambient
Double-tilt, helium [2]	±20	16-300
Double-tilt, nitrogen [2]	±20	90-350
Double-tilt, heating [2]	±20	300-1273
Single-tilt, heating [2]	-	300-1573
Single-tilt, heating, strain [1]	-	300-1000(?)
Single-tilt, Faraday cup [1]	-	ambient

1) JEOL Ltd., 2) Gatan Inc.

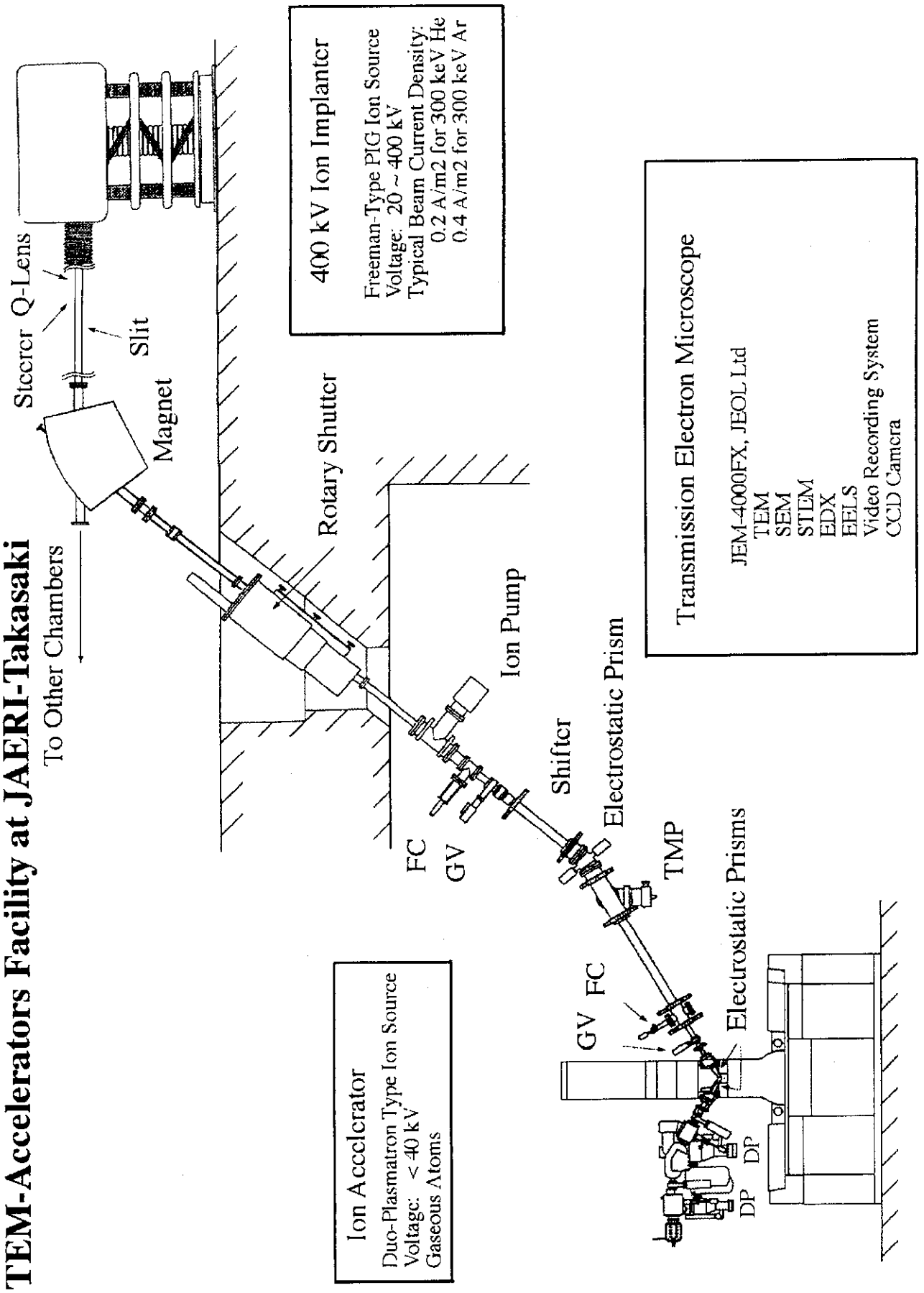

Figure 1. A schematic diagram of the TEM-Accelerators Facility.

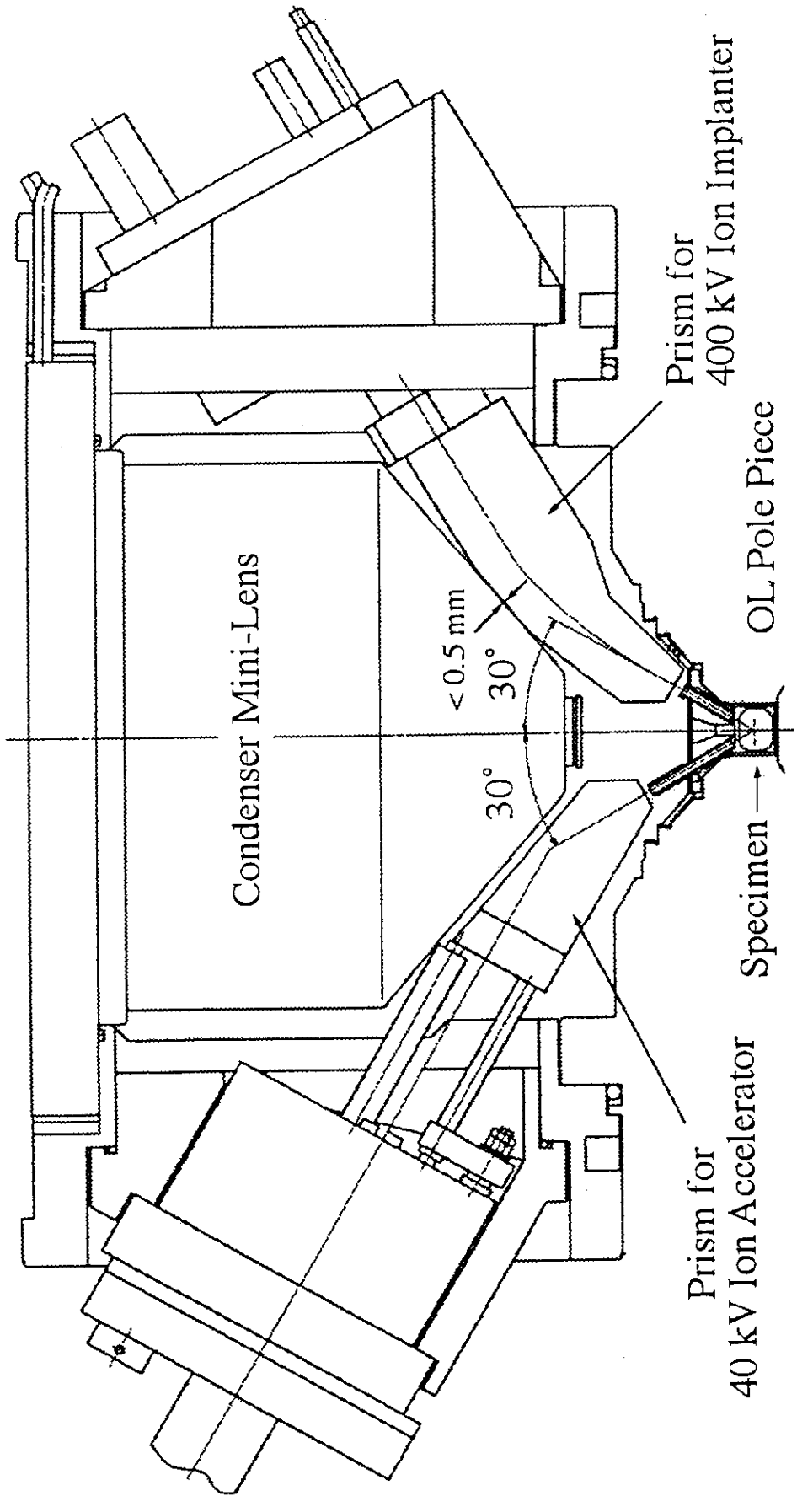

Figure 2. A schematic diagram showing a vertical view of the inside of the TEM specimen chamber.

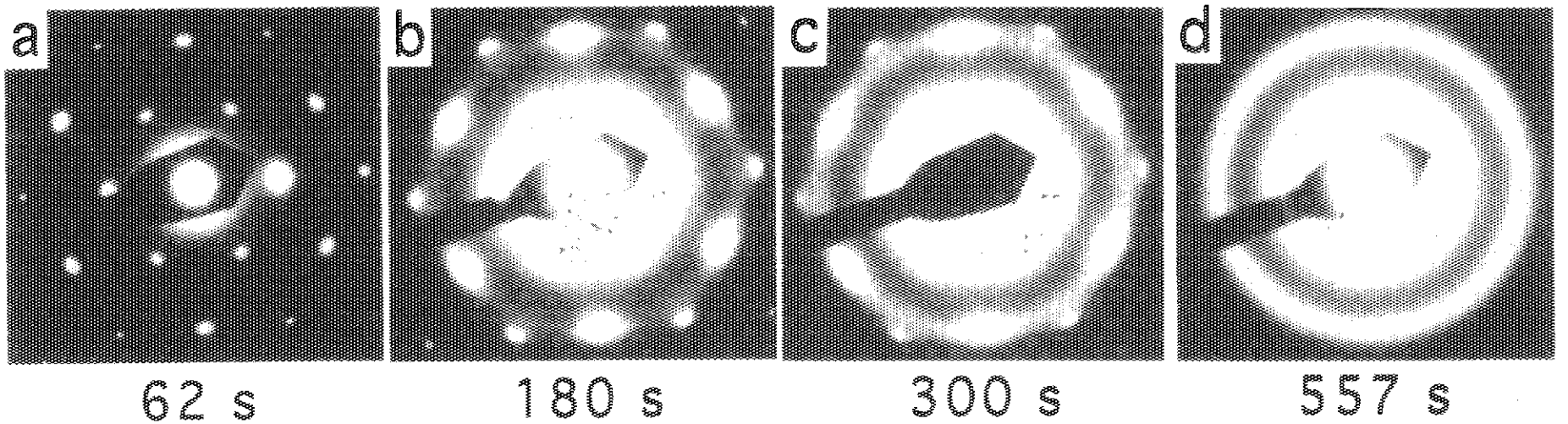

Figure 3. A sequence of selected area electron diffraction patterns, showing amorphization process in graphite irradiated with 40 fJ (250 keV) carbon ions at 573 K. Flux and dose rate are 4.6×10^{19} ions/m^{2}s and 7.8×10^{-4} dpa/ions, respectively.

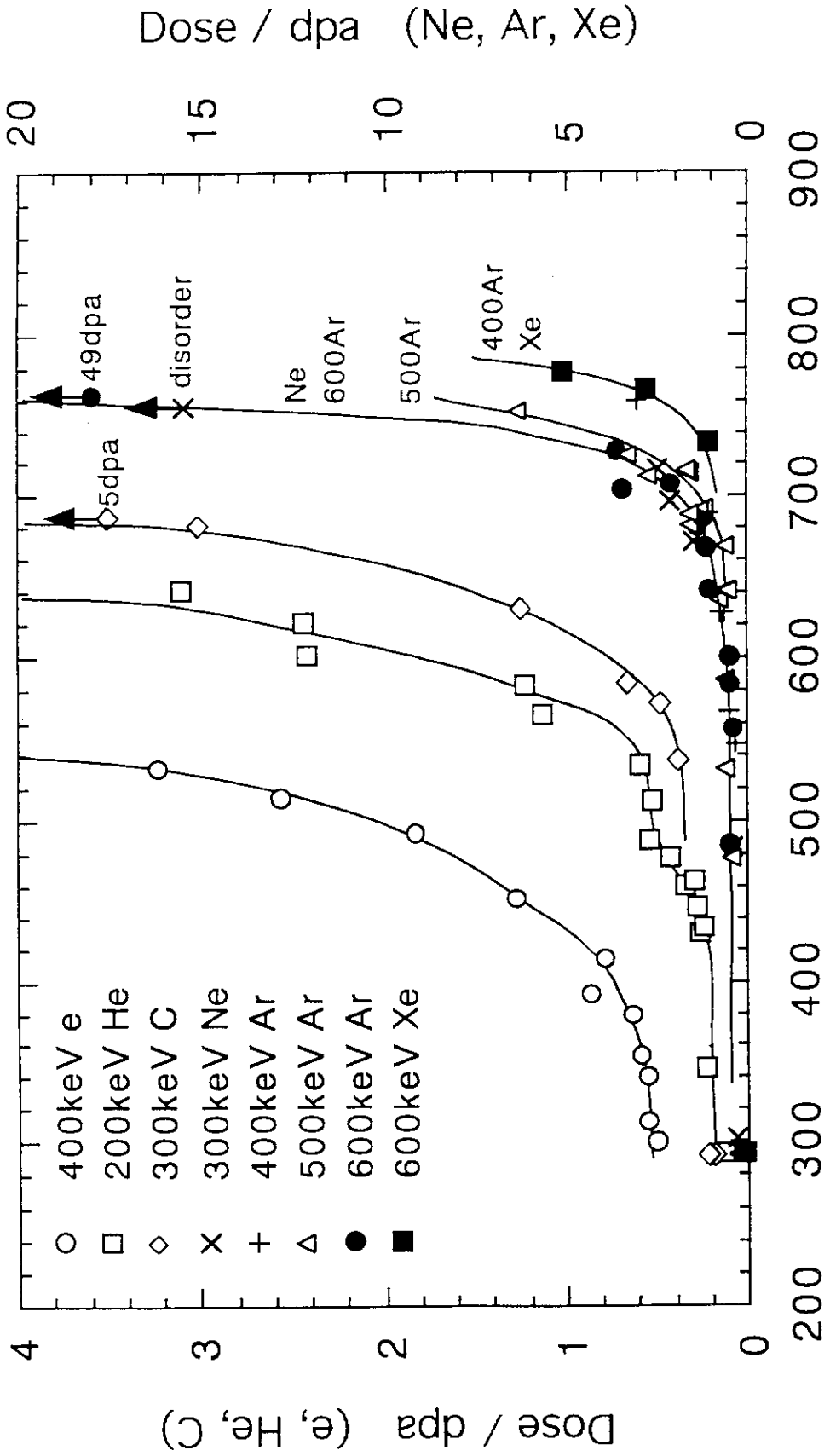

Figure 4. Temperature dependence of the dose-to-amorphization under various kinds of projectile conditions in graphite.

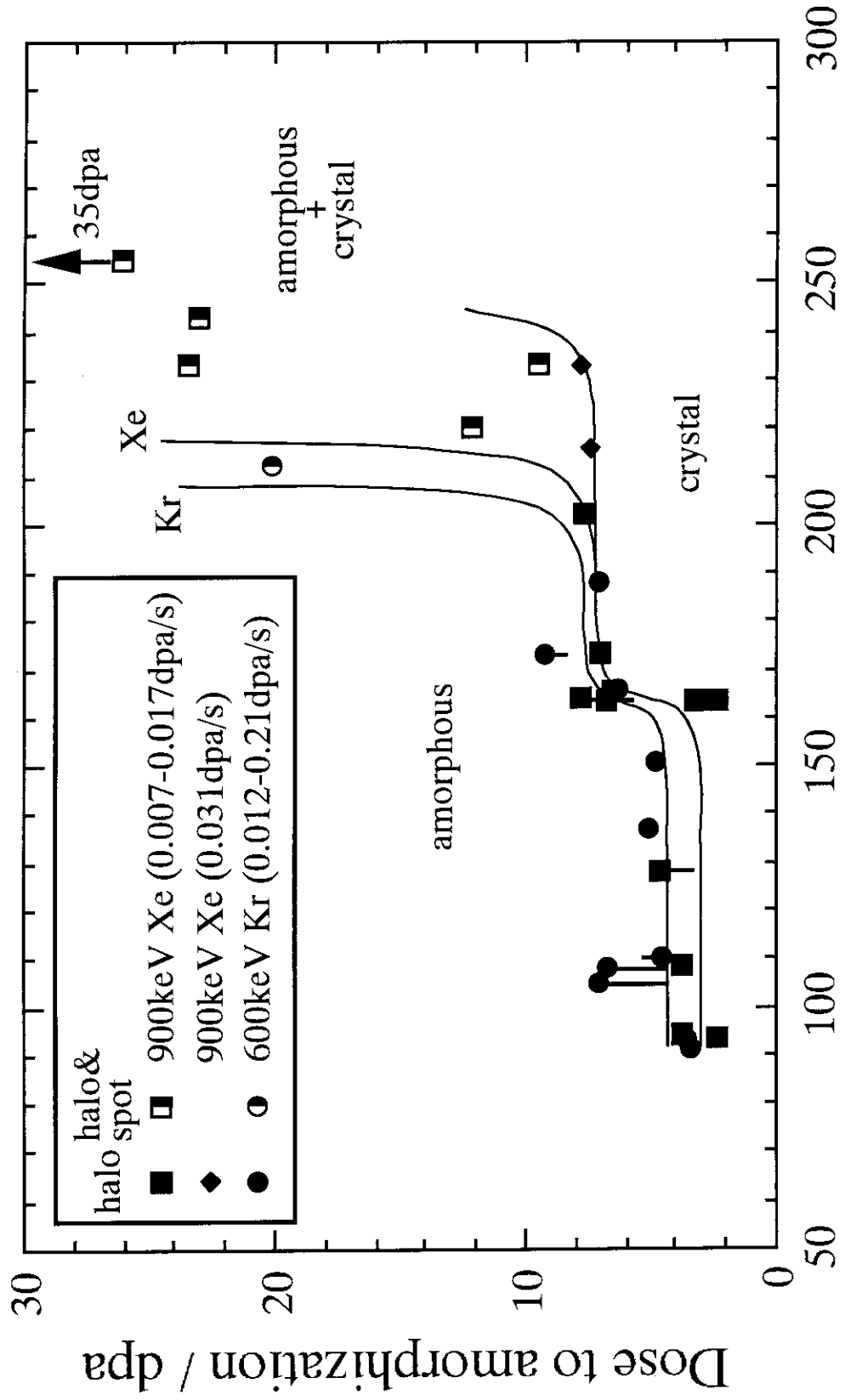

Figure 5. Temperature dependence of the dose-to-amorphization under irradiation with xenon and krypton ions in alpha-alumina.

Note that no amorphization was detected under irradiations with argon and oxygen ions.

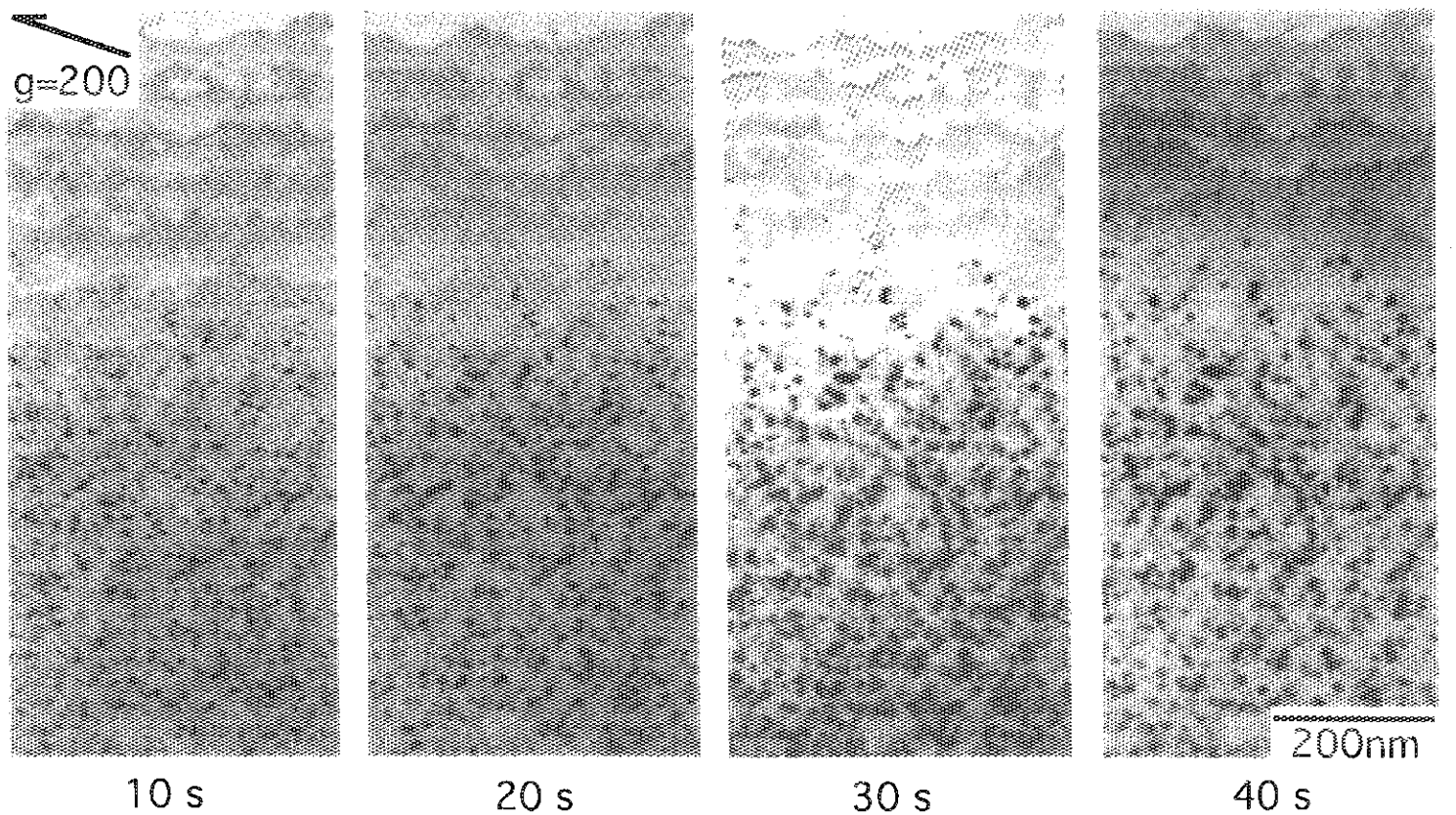

Figure 6. A sequence of bright field images, showing damage evolution process in magnesia irradiated with 16 fJ (100 keV) O^+ ions at 1010 K. Flux of ions is 1.7×10^{17} ions/m^2s, while dose rate varies from 0.0015 to 0.0026 dpa/s depending on specimen thickness.

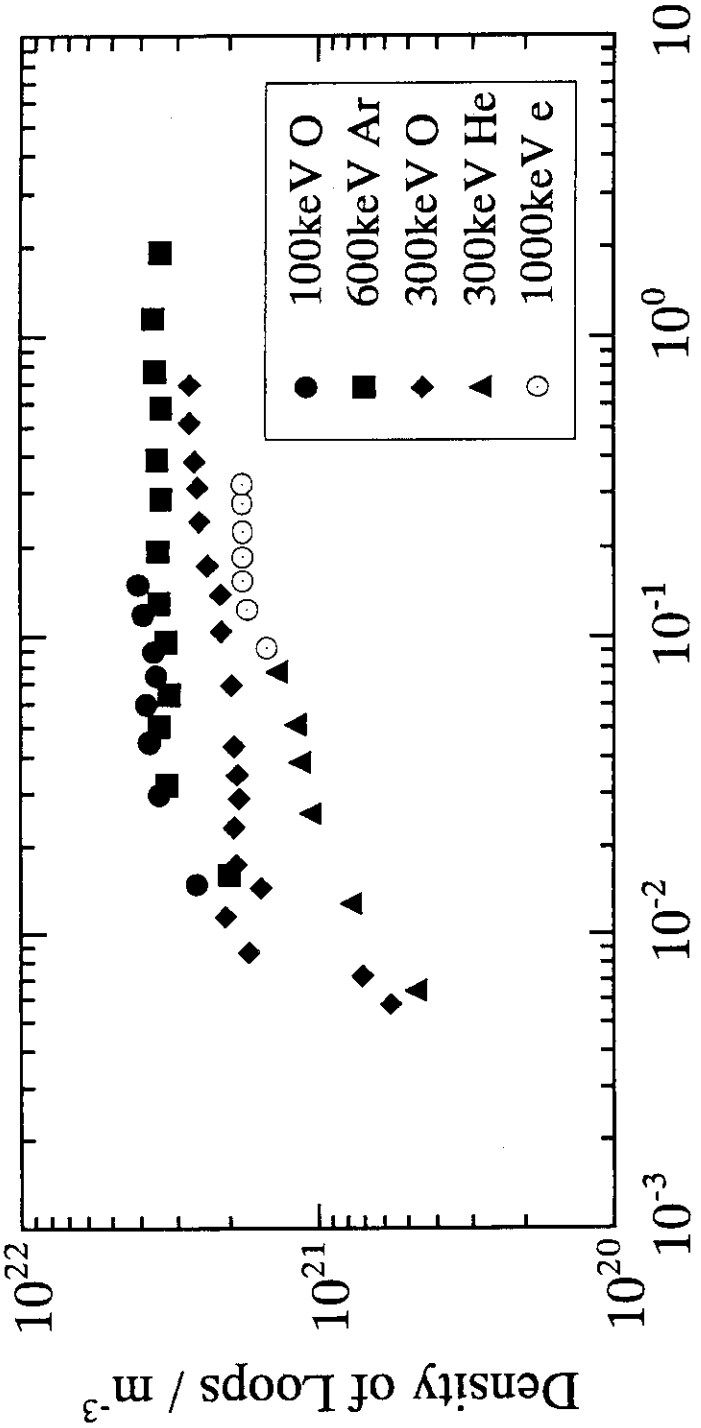

Figure 7. Variation in volume density of dislocation loops in magnesia under irradiation with ions or electrons.